Sensors and Actuators B 202 (2014) 1010–1018

Contents lists available at ScienceDirect

Sensors and Actuators B: Chemical

journal homepage: www.elsevier.com/locate/snb

The ethanol-sensing properties of porous GaN nanofibers synthesized by electrospinning

Xiaoju Luo [a], Xuejun Zheng [a,b,*], Ding Wang [a], Yong Zhang [b], Hongbin Cheng [a], Xianying Wang [a], Huaijuan Zhuang [a], Yanlou Lou [a]

[a] College of Materials Science and Engineering, University of Shanghai for Science & Technology, Shanghai 200093, People's Republic of China
[b] Faculty of Materials, Optoelectronics and Physics, Xiangtan University, Xiangtan, Hunan 411105, People's Republic of China

ARTICLE INFO

Article history:
Received 3 February 2014
Received in revised form 31 May 2014
Accepted 13 June 2014
Available online 20 June 2014

Keywords:
Gallium nitride
Porous structures
Electrospinning
Ethanol sensing properties

ABSTRACT

Through precursor, subsequent calcination and ammoniation, gallium nitride nanofibers (GaN-NFs) and gallium nitride nanoparticles (GaN-NPs) were synthesized by electrospinning and sol–gel method, respectively. The structure and morphology characteristics of the products were investigated by X-ray diffraction (XRD), field-emission scanning electron microscopy (FESEM), energy dispersive X-ray spectroscopy (EDS), X-ray photoelectron spectroscopy (XPS), transmission electron microscopy (TEM) and Brunauer–Emmett–Teller (BET) nitrogen adsorption–desorption measurements. Gas sensors were fabricated as side-heated structure. The ethanol sensing properties of the GaN-NFs and GaN-NPs were compared at operating temperatures from 280 to 360 °C and ethanol concentrations ranging from 50 to 1000 ppm. The results indicate that the porous GaN-NFs show improved response to ethanol with good selectivity, which is attributed to the 1D porous nanostructure. The ethanol sensing mechanism of the porous GaN-NFs was also discussed.

1. Introduction

Recent years, nanostructures of various materials have attracted considerable interest from researchers due to their high performance as the chemical sensing materials [1]. The reliable and portable gas sensors can detect harmful gases in real time with high sensitivity and selectivity, and the sensor's development is extremely important [2]. Electrospinning is a relatively simple and versatile method to fabricate nanofibers with diameters in the range of nanometers to a few micrometers [3]. The high surface-to-volume ratio, high porosity and other outstanding properties make the electrospinning nanofibers being widely used as templates to fabricate various hierarchical nanostructures for sensors, catalysts, remediation and pollution control applications [4–7]. Especially, the nanostructures synthesized by electrospinning have been proved to be quite potential for gas sensors, because the large surface-to-volume ratio and high porosity are beneficial for gas diffusion and mass transport in sensor materials, thus leading to an improved sensing performance [8–11].

GaN is a wide-band-gap semiconductor (3.4 eV at 300 K), and it is known to be a promising material for chemical sensor applications with remarkable properties including excellent chemical stability and biocompatibility [12,13]. As was demonstrated, various reducing and oxidizing gases like carbon monoxide (CO), hydrogen (H_2), acetylene (C_2H_2) and nitric oxides (NO and NO_2) can be tested using heterostructured GaN thin films [14–16], hydrogen (H_2) and nitrogen dioxide (NO_2) can be detected using GaN nanowires in previous researches [1,17,18]. Up to now, a series of electronic and optical devices based on GaN-NFs such as UV photodetector has been fabricated [19], however, to the best of our knowledge, relatively few reports on the gas sensing properties of GaN-NFs are available in the literatures.

Through precursor, subsequent calcination and ammoniation, gallium nitride nanofibers (GaN-NFs) and gallium nitride nanoparticles (GaN-NPs) were synthesized by electrospinning and sol–gel method, respectively, and microstructure, morphology, phase composition, surface area, and pore size of the GaN-NFs and GaN-NPs were investigated by X-ray diffraction (XRD), field-emission scanning electron microscopy (FE-SEM), energy dispersive X-ray spectroscopy (EDS), X-ray photoelectron spectroscopy (XPS), transmission electron microscopy (TEM) and volumetric adsorption analyzer. The nitrogen adsorption–desorption and pore size distribution measurements were carried out using volumetric adsorption analyzer. It is known that gas sensing properties are

* Corresponding author at: College of Materials Science and Engineering, University of Shanghai for Science & Technology, Shanghai 200093, People's Republic of China. Tel.: +86 021 55270588; fax: +86 021 55270588.
E-mail address: zhengxuejun@usst.edu.cn (X. Zheng).

http://dx.doi.org/10.1016/j.snb.2014.06.040
0925-4005/

strongly related to the microstructure of the material such as grain size, shape and porous effects [20]. The GaN-NFs and GaN-NPs are of similar grain sizes due to the same precursor in electrospinning and sol–gel method, and the effects on ethanol sensing properties are considered excluding the possible grain size effect as a primary research. In next step, the ethanol sensing properties will be focused on comparing GaN-NFs and GaN nanowires to exclude the possible shape effect, after GaN nanowires with the similar shape of the GaN-NFs have been obtained. The response on temperature and selectivity measurements were performed to determine the optimum operating temperature and the selected gas with the highest response among the ten target gases by using gas-sensing analysis system. The response value, response time and recovery time are analyzed through the response–recovery characteristic curves, in order to know whether the porous GaN-NFs show improved response to ethanol with good selectivity. The ethanol sensing mechanism is discussed via the attribution of surface-to-volume ratio from the porosity and 1D nanofiber structure. We expect the researches may offer useful guidelines to understand and employ the porous GaN-NFs for gas sensors.

2. Experimental

2.1. Preparations of the GaN-NFs and GaN-NPs

All the chemicals were analytical grade from Aladdin Reagent (Shanghai) Co., Ltd. and used without further purification. In a typical procedure, after an appropriate amount of gallium (III) nitrate hydrate ($Ga(NO_3)_3{\cdot}xH_2O$) was dissolved in deionized water and ethanol with the mass ratio of $Ga(NO_3)_3{\cdot}xH_2O$, deionized water and ethanol 1:4:4, polyvinylpyrrolidone (PVP, M_W = 1,300,000 g mol^{-1}) was added to form a uniform and translucent precursor under vigorous stirring. The precursor was loaded into a plastic syringe with a stainless steel nozzle which is positioned at a fixed distance from a metal cathode as collector, then it was electrospun into composite nanofibers with a computer-controlled syringe pump and an applied voltage of 20 kV between the electrospinning nozzle and the collector. After PVP template and nitrates were decomposed by annealing at 900 °C for 2 h with a heating rate of 2 °C min^{-1} for the composite nanofibers, they became as the white Ga_2O_3 nanofibers (Ga_2O_3-NFs). The Ga_2O_3-NFs were ammoniated at the temperature of 850 °C for 2 h with the same heating rate of 2 °C min^{-1} in a flow of 200 sccm NH_3, and they were finally synthesized as the yellow GaN-NFs. GaN-NPs were prepared by sol–gel from the same precursor. The precursor was put in the oven for 5 h at 60 °C to remove water and ethanol. After that, GaN-NPs were obtained by annealing at 900 °C for 2 h in the air and then ammoniating at 850 °C for 2 h in a flow of 200 sccm NH_3.

2.2. Characterization of materials

The crystal structures of the GaN-NFs and GaN-NPs were determined by XRD (Bruker, D8 Advance, Germany) with Cu-Kα (λ = 0.15418 nm) radiation in the range of 20–80° at room temperature. The morphology and elementary composition were investigated via SEM image and EDS pattern obtained by FE-SEM (FEI, Quanta FEG 450, USA), and the porous microstructure was confirmed by TEM (JEOL, JEM 2100F, Japan). The composition information was further investigated by XPS (TMO, ESCALAB 250 Xi, England), and the position of the C 1s peak (284.5 eV) was used to correct the XPS binding energies. The nitrogen adsorption–desorption isotherms and pore size distribution curves were measured by using fully automated, surface area and porosity analyzer (MI, Tristar II 3020, USA).

2.3. Fabrication of sensors

The gas sensors with sensing and heating elements were fabricated. At first, the GaN-NFs or GaN-NPs were mixed with deionized water in an agate mortar to form a homogeneous paste, and it was coated on a ceramic tube with a pair of gold electrodes attached with Pt wires. After the tube was dried at 80 °C for 2 h to remove water, a Ni–Cr heating wire, which is used to control the operating temperature for sensor was inserted into the tube to form a gas sensor. There is a schematic drawing of an as-fabricated gas sensor as shown in Fig. 1a. Finally, the ceramic tube and heating wire were then welded onto a pedestal with six probes to get the gas sensor in Fig. 1b.

2.4. Measurement of sensors

The sensing properties of the GaN-NFs and GaN-NPs were measured by using the intelligent gas sensing analysis system (Beijing Elite Tech Co., Ltd., CGS-8, China), which consists of gas sensing test equipment and gas distribution systems. A static testing system was used to research the sensing properties, and the different concentrations of vapors were obtained by injecting liquid or gas of volume Q into a testing chamber. The volume Q can be determined by

$$Q = \frac{V \times C \times M}{22.4 \times d \times \rho} \times 10^{-9} \times \frac{273 + T_R}{273 + T_B} \quad (1)$$

$$Q = V \times C \quad (2)$$

Here, V, C, M, d, ρ, T_R, and T_B are the test chamber volume, vapor concentration (ppm), molecular mass, liquid density, liquid purity, environmental temperature, and temperature in the testing chamber, respectively. The volume Q is determined by Eq. (1) for liquid and Eq. (2) for gas. The background gas is air. The response of the sensor to a target gas is defined as R_a/R_g, where R_a and R_g are the sensor resistances in air and the target gas, respectively. The time taken by the resistor to range from R_a to $R_a - 90\%(R_a - R_g)$ is defined as the response time, when the sensor is exposed to the target gas. The time taken by the resistor to change from R_g to $R_g + 90\%(R_a - R_g)$ is defined as the recovery time, when the sensor is retrieved from the target gas [21]. The responses to 100 ppm ethanol for GaN-NFs and GaN-NPs sensors were measured at the different operating temperatures at the range of 280–360 °C, and they will be used to determine the optimum operating temperature. In selectivity measurement, the responses to 100 ppm different gases, such as methanol, acetone, benzene, formaldehyde, ethanol, hydrogen, i-butane, methane, carbon monoxide and ammonia, were performed at the optimum operating temperature for the GaN-NFs and GaN-NPs sensors. The response–recovery characteristic curves were detected at the optimum operating temperature and the ethanol concentration range of 50–1000 ppm. To investigate the selectivity at different operating temperatures, the GaN-NFs sensor responses to 100 ppm of different gases at different temperatures were tested.

3. Results and discussion

3.1. Crystalline structure

XRD patterns of Ga_2O_3-NFs before ammoniation and GaN-NFs after ammoniation are shown in Fig. 2a in order to trace the ammoniating reaction. The diffraction peaks of Ga_2O_3 before ammoniation can be indexed as monoclinic structure Ga_2O_3 (or β-Ga_2O_3), which is consistent with the reported data (JCPDS No. 41-1103) [22]. The diffraction peaks of GaN-NFs after ammoniation agree well with hexagonal wurtzite structure of GaN (JCPDS No. 50-0792) and no diffraction peak from any other impurities

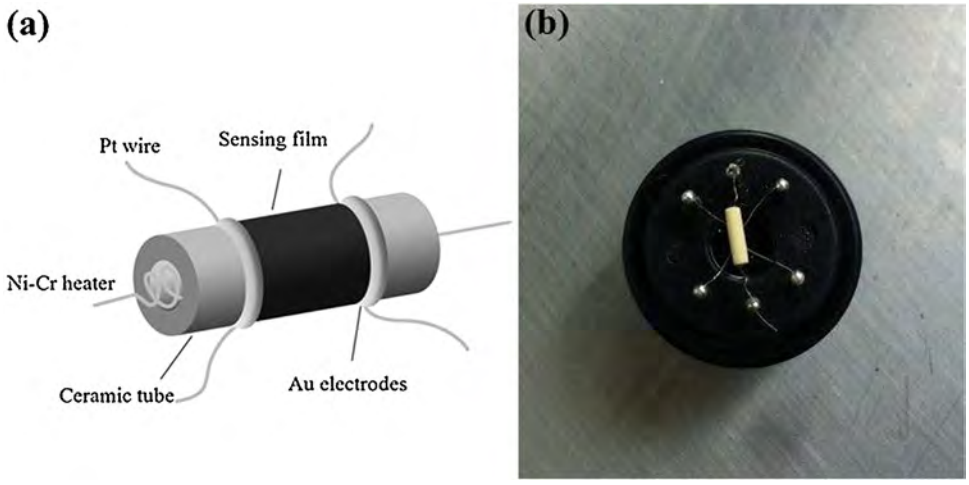

Fig. 1. (a) Schematic structure and (b) the photograph of the gas sensor.

such as Ga_2O_3 was observed from the pattern, which confirms the superb purity of the GaN-NFs [22]. It is concluded that β-Ga_2O_3 turns into GaN after ammoniation at 850 °C for 2 h. The reaction equation can be represented as follows:

$$Ga_2O_3 + 2NH_3 \rightarrow 2GaN + 2H_2O \quad (3)$$

To verify the function of electrospinning, the GaN-NPs were also prepared for comparison by using the same precursor and process, and XRD patterns of the as-prepared products are shown in Fig. 2b. The peaks of GaN-NPs can be indexed as pure wurtzite structure of GaN (JCPDS No. 50-0792). Furthermore, the average crystallite size was calculated from X-ray line broadening analysis based on the Scherrer equation $D = 0.89\lambda/(\beta\cos\theta)$, where D, λ, β and θ are the average crystal size in nm, the X-ray wave length ($\lambda = 0.1541$ nm), the full width at half-maximum of the peak, and the corresponding Bragg diffraction angle [23]. The mean crystallite sizes of the GaN-NFs and GaN-NPs are calculated as 19.5 and 19.8 nm. In addition, compared to GaN-NPs, the 0 0 2 peak of the GaN-NFs increases significantly, which corresponds to the orthogonal [0 0 1] growth direction [24].

3.2. Morphologies

The morphologies of Ga_2O_3-NFs before ammoniation and GaN-NFs after ammoniation were imaged by FE-SEM, and they are composed of abundant and homogeneous nanofibers, as shown in Fig. 3a and b. Both of the Ga_2O_3-NFs and GaN-NFs are of the continuous structure, and the diameters of the former are obvious larger than those of the latter. It can be attributed to excessive H_2O produced in the reaction, which may be present in the structure and result in the loose morphology during ammoniation [19].

The EDS and XPS patterns were used to confirm the elemental composition of the GaN-NFs, and they are given in Fig. 4a and b. In Fig. 4a, the N signal is much weaker than Ga signal because the EDS detector has a low sensitivity at the energy corresponding to the N emission [25]. The low sensitivity may lead to a certain amount of error for quantitative analysis, but it is credible for confirming that the GaN-NFs only contain Ga and N elements [1,26]. In Fig. 4b, the atomic ratio is 44:35:21 for the presence elements of Ga, N and O. The deviation for the atomic ratio of Ga and N is attributed to nitrogen vacancies, and the O may be from the chemisorption of oxygen [27].

The morphologies of the GaN-NFs and GaN-NPs were investigated at high magnification by FE-SEM, and they are given in Fig. 5a and b. From the former the crosslinked GaN-NFs are of the

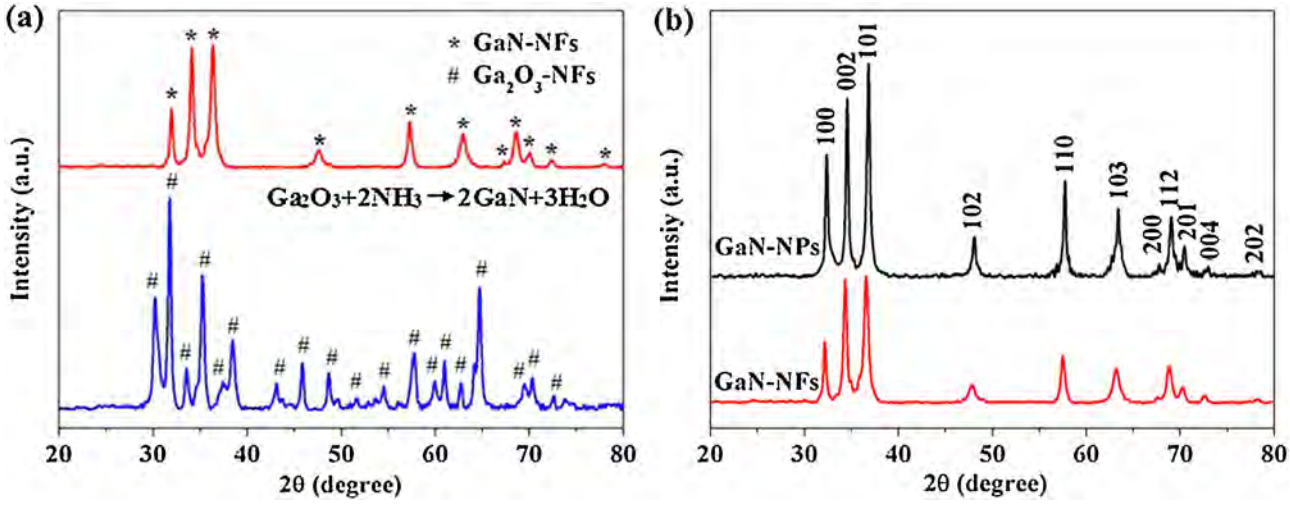

Fig. 2. XRD patterns of (a) Ga_2O_3-NFs before ammoniation and GaN-NFs after ammoniation and (b) GaN-NFs and GaN-NPs for comparison.

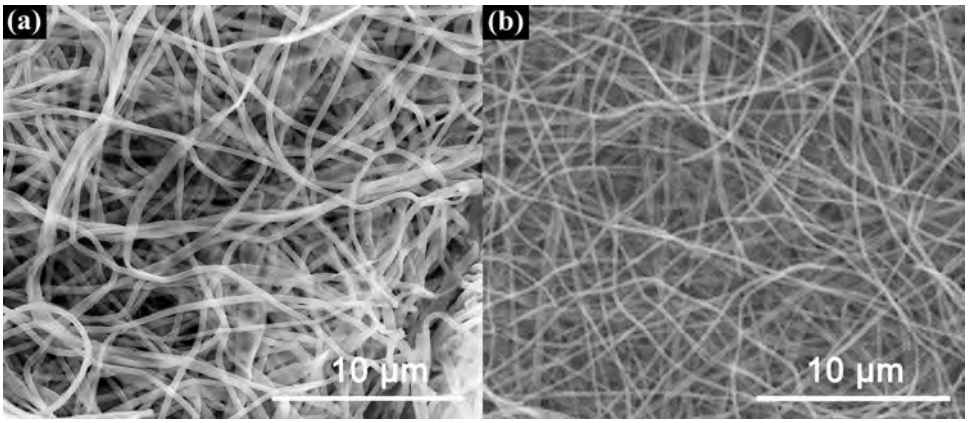

Fig. 3. FE-SEM images of (a) Ga_2O_3-NFs before ammoniation and (b) GaN-NFs after ammoniation.

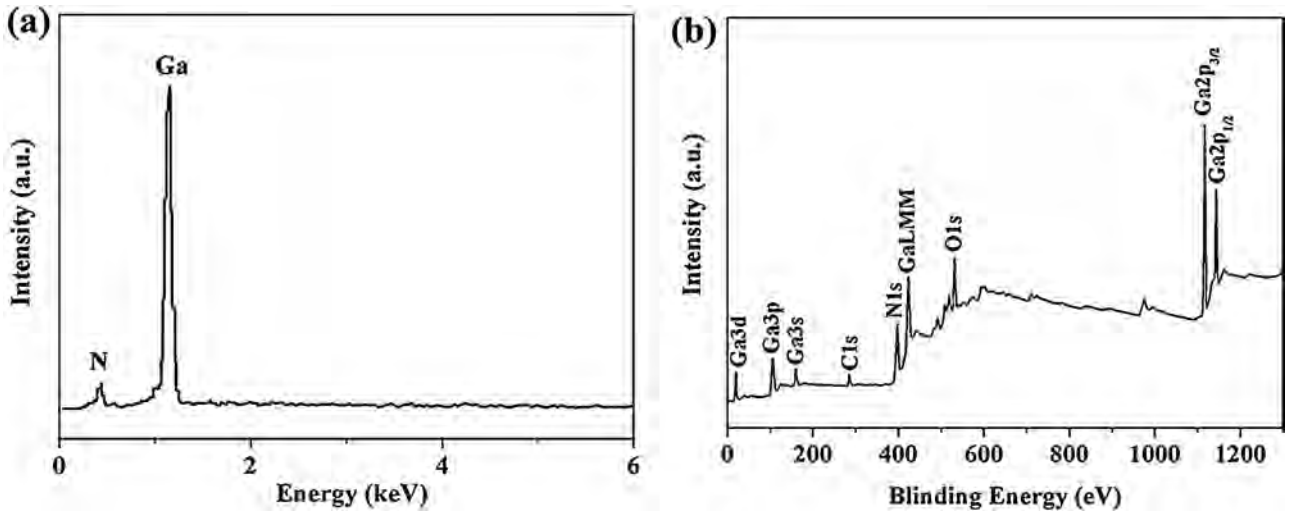

Fig. 4. (a) EDS and (b) XPS patterns of GaN-NFs.

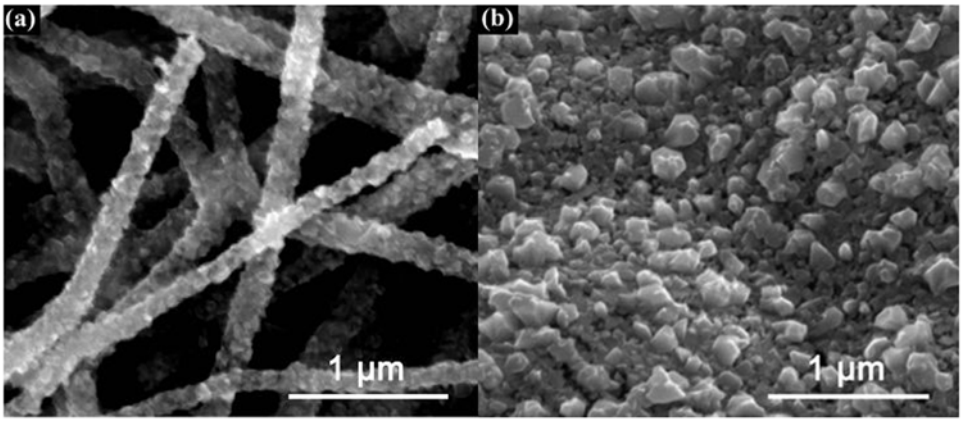

Fig. 5. FE-SEM images of (a) GaN-NFs and (b) GaN-NPs.

diameters at the range of 120–250 nm, and they are made up of crystal grains, faintly. From the latter, the GaN-NPs are of the diameters at the range of 20–100 nm, but one cannot know a clear and definite structure of crystal grains in the GaN-NPs. It is in good agreement with the previous experimental report for TiO_2-NFs and TiO_2-NPs [28]. The porous structures of the single GaN-NF and GaN-NP were further confirmed by TEM, and the morphologies are shown in Fig. 6a and b. From the former the GaN-NF is obviously made up of crystal grains with the diameters about 15–25 nm, and the porous nanofier is of the diameter about 230 nm. In the latter, the GaN-NP is also made up of crystal grains with the diameters about 15–30 nm. They coincide with the mean crystallite size 19.5 and 19.8 nm for the GaN-NFs and GaN-NPs according to the XRD analysis in Fig. 2b. The crystal grains of the single GaN-NF and GaN-NP are similar in both shape and size, because they are obtained by using the same precursor and heat treatment.

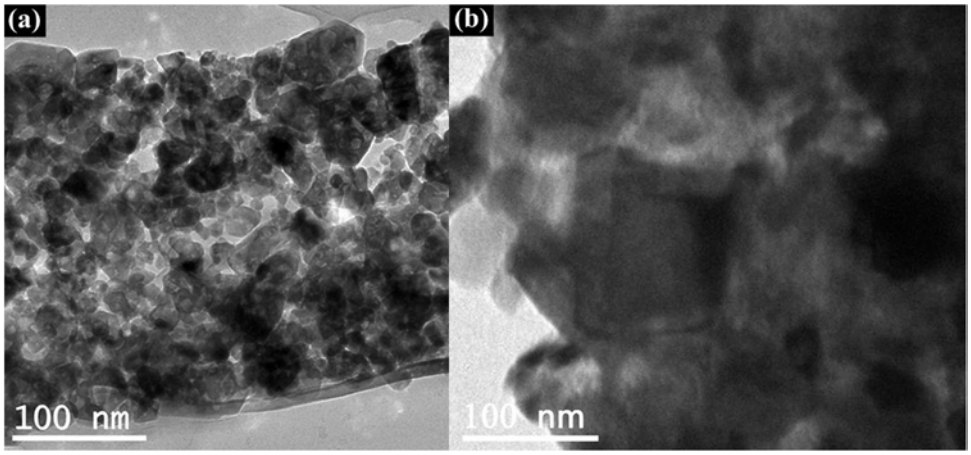

Fig. 6. TEM images of (a) GaN-NFs and (b) GaN-NPs.

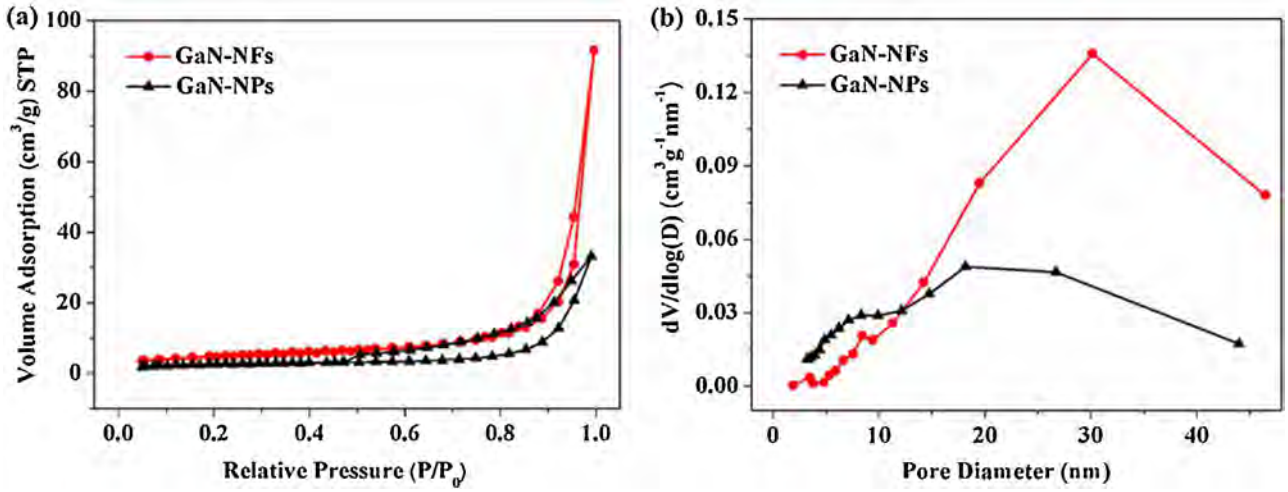

Fig. 7. (a) Typical nitrogen adsorption–desorption isotherms and (b) corresponding pore size distribution curves.

3.3. Specific surface area and pore size distribution

The nitrogen adsorption–desorption isotherms and pore size distribution curves were measured to determine the specific surface area and pore volume of the GaN-NFs and GaN-NPs, and they are presented in Fig. 7a and b. From Fig. 7a, the BET specific surface areas are 17.8 $m^2 g^{-1}$ and 8.2 $m^2 g^{-1}$ for the GaN-NFs and GaN-NPs, and the former is obvious larger than the latter. Both the GaN-NFs and GaN-NPs exhibit type IV isotherms with type H3 hysteresis, which is indicative of mesoporosity [29]. Despite the similar porosity, the pore size distribution curves derived from the desorption data and calculated using the Barret–Joyner–Halenda (BJH) model, show that the average pore diameter 31.8 nm for the GaN-NFs is larger than 24.7 nm for the GaN-NPs in Fig. 7b. It suggests that the mesoporosity of GaN-NFs is improved during the electrospinning process, which is mainly ascribed to the nanofiber structure and polymer-preoccupied space. The large BET surface area and porosity provide efficient transport pathways to their interior voids, which may cause a high response.

3.4. Sensing performance

In order to obtain the optimum operating temperature of gas sensor, the GaN-NFs and GaN-NPs gas sensors were exposed to 100 ppm ethanol at various temperatures, and the response vs. temperature curves are given in Fig. 8. With the temperature increasing, the response value reaches the maximum at 320 °C, then decreases sharply. When the optimum operating temperature was selected as 320 °C, the response values were 8.5 and 4.0 for the GaN-NFs and GaN-NPs sensors. The optimum operating temperature

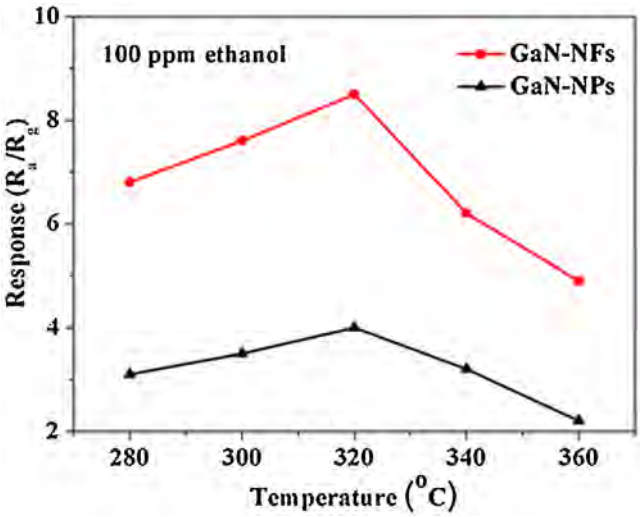

Fig. 8. Responses to 100 ppm ethanol at different operating temperatures.

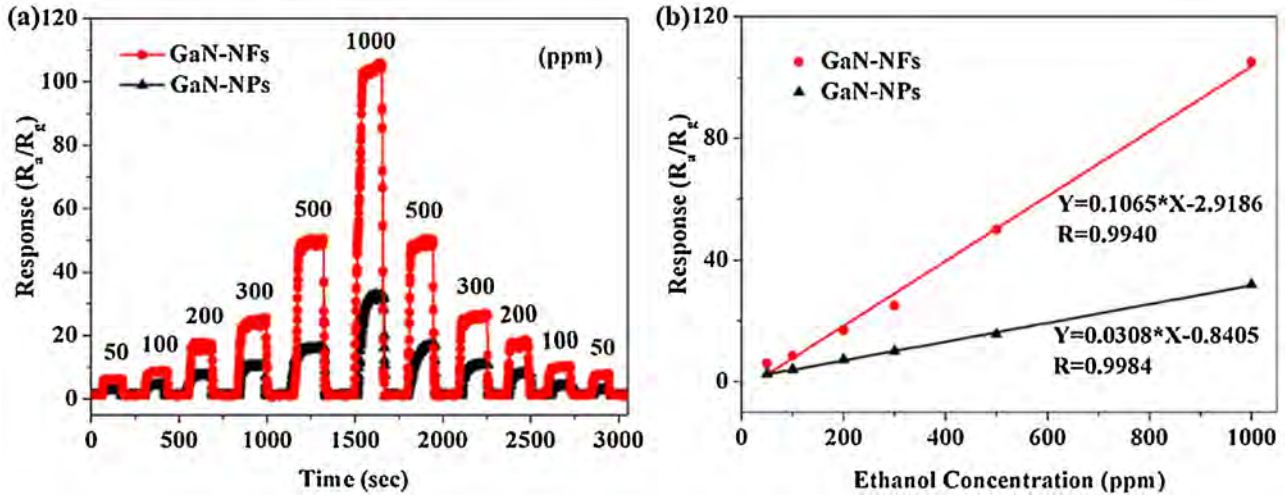

Fig. 9. (a) Response vs. time curves and (b) response vs. ethanol concentration curves of GaN-NFs and GaN-NPs sensors at the range of 50–1000 ppm.

of 320 °C could be applied in all measurements hereinafter. It is in good agreement with the previous report for the gas sensor of GaN nanowires [1].

The response characteristics of the GaN-NFs and GaN-NPs gas sensors were measured at different ethanol concentrations from 50 to 1000 ppm, and the response R_a/R_g vs. time curves are given in Fig. 9a. The response values rise rapidly with increasing the ethanol concentration, indicating that the two sensors still have not become saturated at 1000 ppm, and the response of the GaN-NFs is obviously higher than that of the GaN-NPs. To further investigate the relationship between sensitivity and ethanol concentration, the correlation curves between the concentrations of ethanol and the responses of the gas sensors are fitted, and they are shown in Fig. 9b. The larger the slope the higher the sensitivity, so the GaN-NFs gas sensor with the slope 0.1065 is of higher sensitivity than the GaN-NPs gas sensor with the slope 0.0308. Both the sensors exhibit a nearly linear response to ethanol in the range of 50–1000 ppm, and it indicates that they can be used to detect ethanol gas, quantitatively.

The response–recovery behavior is an important parameter for estimating the gas-sensing properties [30], and the typical response–recovery characteristic curves are given in Fig. 10 for the

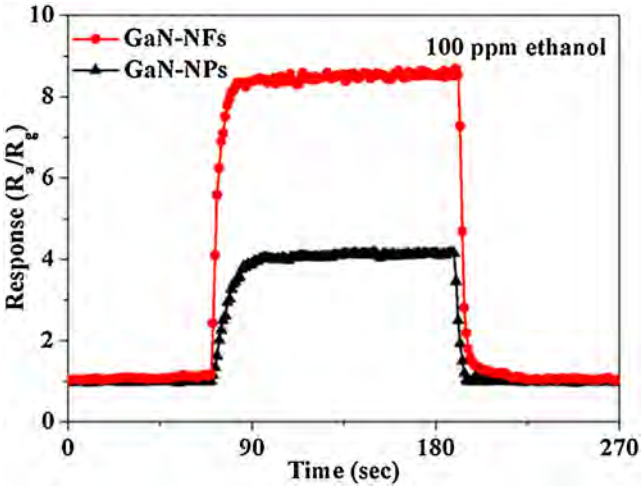

Fig. 10. Typical response–recovery characteristic curves of the sensors to 100 ppm ethanol.

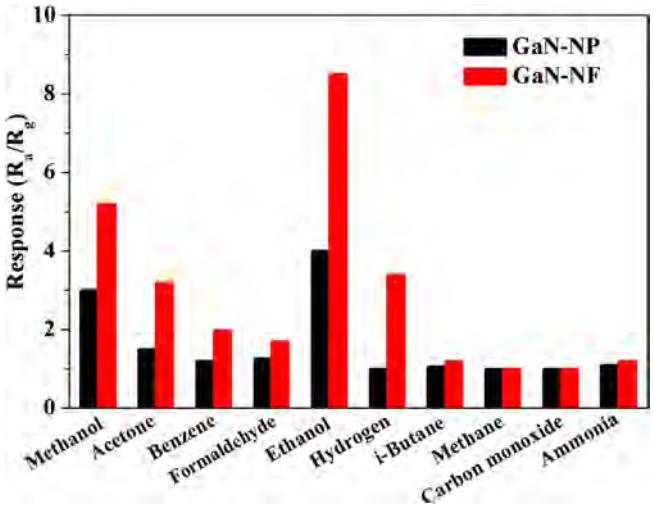

Fig. 11. The GaN-NFs and GaN-NPs sensors responses to 100 ppm of different gases at 320 °C.

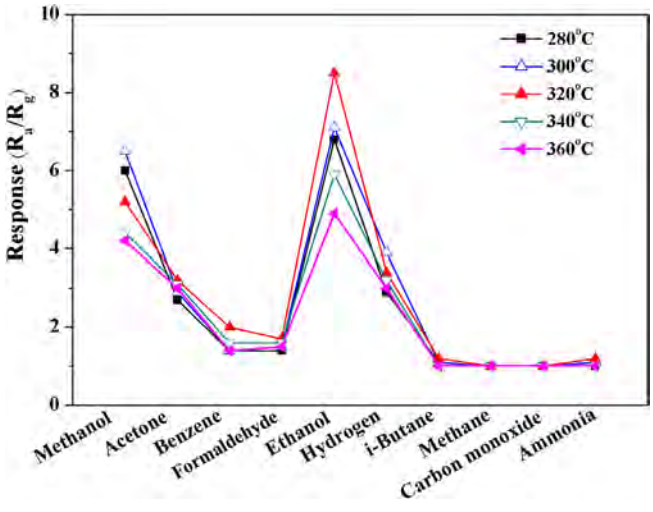

Fig. 12. The GaN-NFs sensor responses to 100 ppm of different gases at different temperatures.

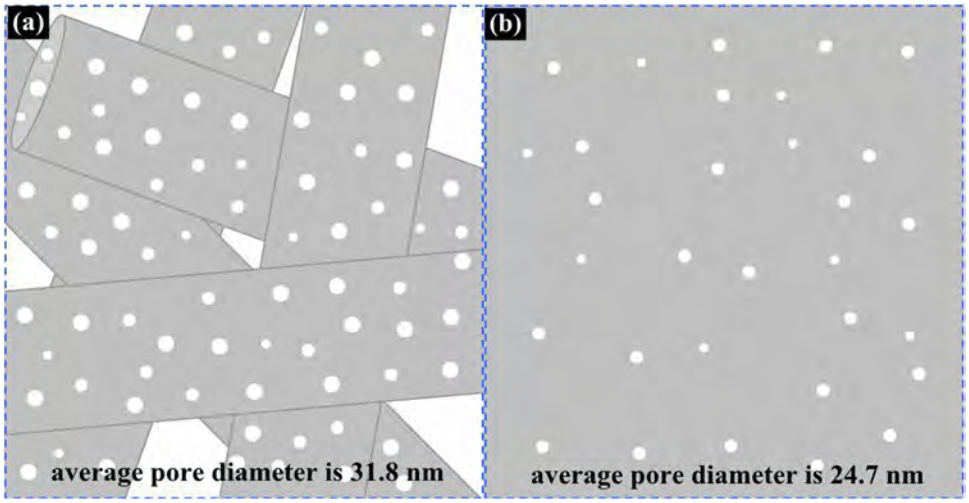

Fig. 13. Schematic diagrams of the gas sensing mechanism of (a) GaN-NFs and (b) GaN-NPs.

sensors to 100 ppm ethanol. The response time and recovery time are 8 s and 5 s for the GaN-NFs sensor and 14 s and 5 s for the GaN-NPs sensor. The recovery times of both sensors are close, but the response time of GaN-NFs is shorter than that of GaN-NPs. It can be attributed to the rapid diffusion of the target gas toward their sensing surface via their porous nanostructures.

The selectivity is a key factor for evaluating practical gas sensors [31], and the sensor responses are given in Fig. 11 for two sensors to 100 ppm of different gases, including methanol (CH_3OH), acetone (C_3H_6O), benzene (C_6H_6), formaldehyde (HCHO), ethanol (C_2H_5OH), hydrogen (H_2), i-butane (C_4H_{10}), methane (CH_4), carbon monoxide (CO) and ammonia (NH_3) at 320 °C. The response values are 5.2, 3.2, 2.0, 1.7, 8.5, 3.4, 1.2, 1, 1 1.2 for the GaN-NFs sensor and 3, 1.5, 1.2, 1.26, 4, 1, 1.06, 1, 1, 1.1 for the GaN-NPs sensor, respectively. Both sensors are much more sensitive to ethanol compared with other gases, and the response of GaN-NFs sensor to ethanol is significantly higher than that of GaN-NPs sensor.

The GaN-NFs sensor responses to 100 ppm of different gases were measured at different temperatures and the results are given in Fig. 12. The responses to gases change with the increasing of temperature from 280 to 360 °C. Obviously, the selectivity to ethanol is dependent on operating temperature, and the highest selectivity is obtained at 320 °C. The operating temperature is one of the most important factors for the material selectivity, as it is based on the sensing reaction energy for different gases [32–34].

3.5. Sensing mechanism

The classical model of an electron depletion layer generated by surface oxygen species is usually considered to be responsible for sensing mechanism of n-type semiconductors, such as ZnO, GaN, ZnS and Ag_2S [35–38]. When the porous GaN-NFs sensor is exposed to the air, oxygen molecules adsorbed on the GaN-NFs surface capture electrons to form chemisorbed oxygen species. The surface potential increases to hinder electron mobility. When the GaN-NFs sensor is exposed to the ethanol gas, the ethanol molecules on the surface react with the surface-adsorbed oxygen ions and return the electron to the nanofibers making the material resistance reduce. The redox reactions taking place on the surface can be schematized as [35]:

$$C_2H_5OH + 3O_2{}^{2-} \rightarrow 2CO_2 + 3H_2O + 6e^- \quad (4)$$

Because the sensing properties are closely related to the gas diffusion and effective surface area, we hope to explain the ethanol-sensing properties of the porous GaN-NFs, particularly the high response and short response time through the important aspects, including the porous structure, large specific surface area and the crosslinked feature between the GaN-NFs [39]. The porous GaN-NFs and GaN-NPs are compared by considering the porous structures in Fig. 6 and the mesoporosity from the pore size distribution curves in Fig. 7, the mechanism of the ethanol-sensing properties is understood via the schematic diagrams Fig. 13a and b for the GaN-NFs and GaN-NPs. First of all, all pores are fully interconnected to form a three-dimensional network in a single GaN nanofiber, and the GaN-NFs are of higher mesoporosity than GaN-NPs in a same volume space. Obviously, the gas in the GaN-NPs cannot spread to the particles in the interior of the aggregate. High mesoporosity of the GaN-NFs is benefit for the gas diffusion toward the entire sensing surface. Secondly, the specific surface area of the GaN-NFs is nearly two times than that of the GaN-NPs after combining with the typical nitrogen adsorption–desorption isotherms, and the improved mesoporosity and the porous structure can enhance effective surface area to adsorb and desorb gas molecules [40]. Finally, compared with the nanoparticles, the nanofibers are of nanoparticle alignment, which could effectively facilitate charge transfer along the nanofiber framework [28], therefore the GaN-NFs have better charge transfer than GaN-NPs. On the other hand, there are more nanofiber–nanofiber junctions of the cross-linked GaN-NFs network on the surface of sensor. Such junctions should form a depleted layer around the intersection, thus the response of the sensor can be attributed to the changes in the resistance of the gas sensor due to both a surface depletion of each nanofiber and the potential barrier height in the junction [41]. The Debye length is defined as the distance over which a local electric field affects the distribution of free charge carriers [42], and a calculation of the Debye length for n-type GaN gives $L_D \leq 100$ nm [43]. The gas response increases abruptly when the grain size becomes comparable to or smaller than the Debye length [44]. The estimated grain sizes for GaN-NFs (19.5 nm) and GaN-NFs (19.8 nm) less than Debye length may be one of the reasons for the high gas responses. To sum up, the improved ethanol-sensing properties of the GaN-NFs can be attributed to the combined actions of the aforementioned items.

4. Conclusion

In summary, the GaN-NFs and the GaN-NPs were synthesized by electrospinning and sol–gel, and the grain size, the crosslinked feature, the porous structure, the composition information and the surface area are confirmed by XRD, FE-SEM, TEM, EDX, XPS and BET for the GaN-NFs. The GaN-NFs sensor exhibits much higher

response, shorter gas response time and better selectivity than those of the GaN-NPs sensor. The optimum operating temperature is 320 °C for the gas sensors to detect ethanol. The recovery times are close for the sensors, but the GaN-NFs sensor is of shorter response time than that of GaN-NPs sensor. The GaN-NFs gas sensor has a higher response to gaseous ethanol than other target gases, and it may be of a potential application in fabricating high performance gas sensors.

Acknowledgments

This work was supported by PCSIRT (IRT1080), NNSF of China (51272158), Changjiang Scholar Incentive Program ([2009]17), and Shanghai Nano Special Foundation (11nm0502600).

References

[1] J. Sim, K. Kim, S. Song, J. Kim, Suspended GaN nanowires as NO_2 sensor for high temperature applications, Analyst 138 (2013) 2432–2437.
[2] L.L. Wang, H.M. Dou, Z. Lou, T. Zhang, Encapsuled nanoreactors (Au@SnO_2): a new sensing material for chemical sensors, Nanoscale 5 (2013) 2686–2691.
[3] Y.E. Miao, S.X. He, Y.L. Zhong, Z. Yang, W.W. Tjiu, T.X. Liu, A novel hydrogen peroxide sensor based on Ag/SnO_2 composite nanotubes by electrospinning, Electrochim. Acta 99 (2013) 117–123.
[4] Q. Guo, J.S. Huang, P.Q. Chen, Y. Liu, H.Q. Hou, T.Y. You, Simultaneous determination of catechol and hydroquinone using electrospun carbon nanofiber modified electrode, Sens. Actuators B 163 (2012) 179–185.
[5] R.Y. Wang, J. Guo, D. Chen, Y.E. Miao, J.S. Pan, W.W. Tjiu, T.X. Liu, Tube brush like ZnO/SiO_2 hybrid to construct a flexible membrane with enhanced photocatalytic properties and recycling ability, J. Mater. Chem. 21 (2011) 19375–19380.
[6] Y.E. Miao, R.Y. Wang, D. Chen, Z.Y. Liu, T.X. Liu, Electrospun self-standing membrane of hierarchical SiO_2@gamma-AlOOH (Boehmite) core/sheath fibers for water remediation, ACS Appl. Mater. Interfaces 4 (2012) 5353–5359.
[7] B. Ding, M.R. Wang, X.F. Wang, J.Y. Yu, G. Sun, Electrospun nanomaterials for ultrasensitive sensors, Mater. Today 13 (2010) 16–27.
[8] X. Yu, F. Song, B. Zhai, C.T. Zheng, Y.D. Wang, Electrospun ZnO nanotubes and its gas sensing applications, Physica E 52 (2013) 92–96.
[9] S.H. Wei, M.H. Zhou, W.P. Du, Improved acetone sensing properties of ZnO hollow nanofibers by single capillary electrospinning, Sens. Actuators B 160 (2011) 753–759.
[10] N.G. Cho, D.J. Yang, M.J. Jin, H.G. Kim, H.L. Tuller, I.D. Kim, Highly sensitive SnO_2 hollow nanofiber-based NO_2 gas sensors, Sens. Actuators B 160 (2011) 1468–1472.
[11] L.L. Wang, X.J. Luo, X.J. Zheng, R. Wang, T. Zhang, Direct annealing of electrospun synthesized high-performance porous SnO_2 hollow nanofibers for gas sensors, RSC Adv. 3 (2013) 9723–9728.
[12] F. Yun, S. Chevtchenko, Y.T. Moon, H. Morkoc, T.J. Fawcett, J.T. Wolan, GaN resistive hydrogen gas sensors, Appl. Phys. Lett. 87 (2005) 073507.
[13] A. Das, A. Das, L.B. Chang, C.S. Lai, R.M. Lin, F.C. Chu, Y.H. Lin, L. Chow, M.J. Jeng, GaN thin film based light addressable potentiometric sensor for pH sensing application, Appl. Phys. Express 6 (2013) 036601.
[14] J. Schalwig, G. Muller, M. Eickhoff, O. Ambacher, M. Stutzmann, Group III-nitride-based gas sensors for combustion monitoring, Mater. Sci. Eng. B 93 (2002) 207–214.
[15] J. Schalwig, G. Muller, M. Eickhoff, O. Ambacher, M. Stutzmann, Gas sensitive GaN/AlGaN-heterostructures, Sens. Actuators B 87 (2002) 425–430.
[16] G.Y. Zhao, W. Sutton, D. Pavlidis, E.L. Piner, J. Schwank, S. Hubbard, A novel Pt-AlGaN/GaN heterostructure Schottky diode gas sensor on Si, IEICE Trans. Electron. E86c (2003) 2027–2031.
[17] W. Lim, J.S. Wright, B.P. Gila, J.L. Johnson, A. Ural, T. Anderson, F. Ren, S.J. Pearton, Room temperature hydrogen detection using Pd-coated GaN nanowires, Appl. Phys. Lett. 93 (2008) 072109.
[18] J.S. Wright, W. Lim, B.P. Gila, S.J. Pearton, J.L. Johnson, A. Ural, F. Ren, Hydrogen sensing with Pt-functionalized GaN nanowires, Sens. Actuators B 140 (2009) 196–199.
[19] H. Wu, Y. Sun, D.D. Lin, R. Zhong, C. Zhang, W. Pan, GaN nanofibers based on electrospinning: facile synthesis, controlled assembly, precise doping, and application as high performance UV photodetector, Adv. Mater. 21 (2009) 227–231.
[20] C.X. Wang, L.W. Yin, L.Y. Zhang, D. Xiang, R. Gao, Metal oxide gas sensors: sensitivity and influencing factors, Sensors 10 (2010) 2088–2106.
[21] D. Wang, P. Hu, J.Q. Xu, X.W. Dong, Q.Y. Pan, Fast response chlorine gas sensor based on mesoporous SnO_2, Sens. Actuators B 140 (2009) 383–389.
[22] J.Y. Li, L. An, C.G. Lu, J. Liu, Conversion between hexagonal GaN and beta-Ga_2O_3 nanowires and their electrical transport properties, Nano Lett. 6 (2006) 148–152.
[23] L.X. Zhang, Y.Y. Yin, Hierarchically mesoporous SnO_2 nanosheets: hydrothermal synthesis and highly ethanol-sensitive properties operated at low temperature, Sens. Actuators B 185 (2013) 594–601.
[24] T. Kuykendall, P.J. Pauzauskie, Y.F. Zhang, J. Goldberger, D. Sirbuly, J. Denlinger, P.D. Yang, Crystallographic alignment of high-density gallium nitride nanowire arrays, Nat. Mater. 3 (2004) 524–528.
[25] J.I. Hong, Y.L. Chang, Y. Ding, Z.L. Wang, R.L. Snyder, Growth of GaN films with controlled out-of-plane texture on Si wafers, Thin Solid Films 519 (2011) 3608–3611.
[26] J. Johnson, Y.H. Choi, A. Ural, W. Lim, J.S. Wright, B.P. Gila, F. Ren, S.J. Pearton, Growth and characterization of GaN nanowires for hydrogen sensors, J. Electron. Mater. 38 (2009) 490–494.
[27] H.D. Xiao, H.L. Ma, C.S. Xue, J. Ma, F.J. Zong, X.J. Zhang, F. Ji, W.R. Hu, Synthesis and structural properties of GaN powders, Mater. Chem. Phys. 88 (2004) 180–184.
[28] S.K. Choi, S. Kim, S.K. Lim, H. Park, Photocatalytic comparison of TiO_2 nanoparticles and electrospun TiO_2 nanofibers: effects of mesoporosity and interparticle charge transfer, J. Phys. Chem. C 114 (2010) 16475–16480.
[29] Y. Zeng, T. Zhang, L.J. Wang, M.H. Kang, H.T. Fan, R. Wang, Y. He, Enhanced toluene sensing characteristics of TiO_2-doped flowerlike ZnO nanostructures, Sens. Actuators B 140 (2009) 73–78.
[30] H. Shan, C.B. Liu, L. Liu, S.C. Li, L.Y. Wang, X.B. Zhang, X.Q. Bo, X. Chi, Highly sensitive acetone sensors based on La-doped alpha-Fe_2O_3 nanotubes, Sens. Actuators B 184 (2013) 243–247.
[31] L.L. Wang, T. Fei, Z. Lou, T. Zhang, Three-dimensional hierarchical flowerlike α-Fe_2O_3 nanostructures: synthesis and ethanol-sensing properties, ACS Appl. Mater. Interfaces 3 (2011) 4689–4694.
[32] L.L. Wang, Z. Lou, T. Fei, T. Zhang, Enhanced acetone sensing performances of hierarchical hollow Au-loaded NiO hybrid structures, Sens. Actuators B 161 (2012) 178–183.
[33] B.H. Jang, O. Landau, S.J. Choi, J. Shin, A. Rothschild, I.D. Kim, Selectivity enhancement of SnO_2 nanofiber gas sensors by functionalization with Pt nanocatalysts and manipulation of the operation temperature, Sens. Actuators B 188 (2013) 156–168.
[34] A. Ponzoni, E. Comini, G. Sberveglieri, J. Zhou, S.Z. Deng, N.S. Xu, Y. Ding, Z.L. Wang, Ultrasensitive and highly selective gas sensors using three-dimensional tungsten oxide nanowire networks, Appl. Phys. Lett. 88 (2006) 203101.
[35] N. Qin, X.H. Wang, Q. Xiang, J.Q. Xu, A biomimetic nest-like ZnO: controllable synthesis and enhanced ethanol response, Sens. Actuators B 191 (2014) 770–778.
[36] Q.N. Abdullah, F.K. Yam, J.J. Hassan, C.W. Chin, Z. Hassan, M. Bououdina, High performance room temperature GaN-nanowires hydrogen gas sensor fabricated by chemical vapor deposition (CVD) technique, Int. J. Hydrogen Energy 38 (2013) 14085–14101.
[37] Z.G. Chen, J. Zou, G. Liu, H.F. Lu, F. Li, G.Q. Lu, H.M. Cheng, Silicon-induced oriented ZnS nanobelts for hydrogen sensitivity, Nanotechnology 19 (2008) 055710.
[38] D.S. Wang, C.H. Hao, W. Zheng, Q. Peng, T.H. Wang, Z.M. Liao, D.P. Yu, Y.D. Li, Ultralong single-crystalline Ag_2S nanowires: promising candidates for photoswitches and room-temperature oxygen sensors, Adv. Mater. 20 (2008) 2628–2632.
[39] G.X. Wang, J.S. Park, M.S. Park, X.L. Gou, Synthesis and high gas sensitivity of tin oxide nanotubes, Sens. Actuators B 131 (2008) 313–317.
[40] C.N. Xu, J. Tamaki, N. Miura, N. Yamazoe, Grain size effects on gas sensitivity of porous SnO_2-based elements, Sens. Actuators B 3 (1991) 147–155.
[41] Q. Qi, T. Zhang, L. Liu, X.J. Zheng, Synthesis and toluene sensing properties of SnO_2 nanofibers, Sens. Actuators B 137 (2009) 471–475.
[42] N. Ramgir, N. Datta, M. Kaur, S. Kailasaganapathi, A.K. Debnath, D.K. Aswal, S.K. Gupta, Zinc oxide nanowires for gas sensing application, Tech. Phys. Div. 325 (2012) 28–33.
[43] P.M. Bridger, Z.Z. Bandic, E.C. Piquette, T.C. McGill, Measurement of induced surface charges, contact potentials, and surface states in GaN by electric force microscopy, Appl. Phys. Lett. 74 (1999) 3522–3524.
[44] L.L. Wang, Z. Lou, T. Fei, T. Zhang, Zinc oxide core–shell hollow microspheres with multi-shelled architecture for gas sensor applications, J. Mater. Chem. 21 (2011) 19331–19336.

Biographies

Xiaoju Luo received her BS degree in environment engineering in 2012 from Wuhan Institute of Technology. She has been pursuing her MS degree in environment engineering in University of Shanghai for Science & Technology since 2012. Now, her research interest is focused on the preparation of GaN nanomaterials and potential application of GaN in gas sensors.

Xuejun Zheng received his MS degree in major of structure mechanics in 1989, and PhD degree in the field of fundamental mechanics in 2002 from Xiangtan University. He was appointed a full professor in Faculty of Materials Optoelectronics and Physics, Xiangtan University in 2003. Now, he is interested in the field of sensing functional materials, gas sensors and humidity sensors.

Ding Wang received his PhD degree in the field of nano-functional materials in 2013 from Toyama University in Japan. Now, he was a teacher of University of Shanghai for Science & Technology. His research interests focused on sensing materials and catalysis.

Yong Zhang received his MS degree in major of materials physics and chemistry in 2007, and PhD degree in the field of materials science and engineering in 2012 from Xiangtan University.

Hongbin Cheng received his M.S. degree from Tsinghua university in 1998 and PhD degree of mechanical engineering from Pittsburg university in 2009. He is now an associate professor of School of materials science and engineering, University of Shanghai for Science & Technology. His research interests focused on functional nanomaterials, MEMS and sensors.

Xianying Wang received her PhD degree of materials science from Shanghai Institute of Optics and Fine Mechanics, Chinese Academy of Sciences in 2005. She is now a professor of School of materials science and engineering, University of Shanghai for Science & Technology. Her research interests focused on semiconducting nanomaterials and related nanodevices.

Huaijuan Zhuang received her BS degree in environment engineering in 2013 from Anhui Normal University. She has been pursuing her MS degree in environmental science in University of Shanghai for Science & Technology since 2013.

Yanlou Lou received his BS degree in environment engineering in 2013 from Yangtze University. He has been pursuing his MS degree in environmental science in University of Shanghai for Science & Technology since 2013.